2014 IEEE International Conference on Robotics & Automation (ICRA)
Hong Kong Convention and Exhibition Center
May 31 - June 7, 2014. Hong Kong, China

Experimental Study on Efficient Use of Singular Configuration in Pulling Heavy Objects with Two-link Robot Arm

Takateru Urakubo, Hiroki Yoshioka, Tomoaki Mashimo and Xianglong Wan

Abstract— **This paper demonstrates that singular configuration of a two-link robot arm is advantageous in doing the task of pulling or lifting up a heavy object with small joint torques. As a result of numerical optimization, the initial configuration that minimizes the joint torques necessary for the task is close to the singular configuration where the arm is stretched out. The singular configuration has the dynamic feature that the joint angle vector can be accelerated in a certain direction almost independently of the mass of the object. Then, the joint torques can generate large kinetic energy efficiently at the singular configuration, and the energy can be utilized to pull or lift up the object. The experimental results show that the dynamic feature is practically useful, even when a feedback control is applied in order to make the object follow a planned trajectory.**

I. INTRODUCTION

In factories, industrial robots are working every day to do various tasks such as moving heavy objects and assembling several components. In near future, robots will work even in unknown environments such as home and disaster areas. Especially, pulling or lifting heavy objects is one of the tasks that the robots are expected to do instead of us. In those environments, the mass of the objects that the robots should handle is also unknown. When motion planning for robots is performed only based on kinematics, the planned motion could be infeasible because necessary joint torques could exceed the maximum torques. In order to increase the number of tasks that a robot can achieve within the maximum torques, the motion planning that reduces the necessary torques is required [1].

Singular configurations of a robot arm are the postures where the Jacobian matrix relating the joint velocities to the velocity of the end effector is singular [2]-[7]. For a two-link robot arm, the posture where the arm is stretched out or folded completely is a singular configuration. Since motion planning through singular configurations is difficult due to the kinematic singularity [8]-[14], singular configurations tend to be avoided for robotic manipulation. However, humans use singular configurations well in their motion such as pulling a heavy object and walking [15].

In the statics, it is well known that singular configurations have an advantage in sustaining a load [16]-[19]. A robot arm can sustain a large load with small joint torques near singular configurations. By using the advantage, the arm near singular configurations can transmit the translational moment with small joint torques from the robot base to the object grasped by the end effector or vice versa [20].

In the dynamics, we have shown that the joint torques can generate kinetic energy most efficiently at singular configurations when a two-link arm pulls a heavy object [21]. The joint torques can accelerate the joint angles almost independently of the mass of the object at singular configurations and generate kinetic energy of the arm. The energy is transmitted to the object through the link mechanism. This dynamic feature of singular configurations can make the arm pull the object with small joint torques. In [21], the optimal motion that minimizes the integral of squared joint torques during the task of pulling a heavy object has been found by numerical optimization. The initial configuration of the arm for the optimal motion is close to the singular configuration where the arm is stretched out.

In this paper, we show through experimental results that the dynamic feature shown in [21] is useful even for the practical tasks of pulling a heavy object. The optimal solution in [21] was obtained under the assumption where no frictional forces act on the robot arm or the object. The frictional forces for the robot arm that we developed for this study are estimated from the results of preliminary experiments, and the numerical optimization is recalculated with the frictional forces. In order to make the end effector follow the planned path accurately, feedback torques are added to the joint torques that are obtained from the motion planning. The experimental results show that, even under the frictional forces and the feedback torques, the task of pulling a heavy object can be achieved with small joint torques when the initial configuration is close to the singular one where the arm is stretched out.

II. OPTIMAL MOTION PLANNING

In this paper, we consider a motion planning problem for a two-link robot arm and solve it by numerical optimization, in a similar way as in [21].

A. Problem Formulation

We suppose that a two-link robot arm pulls or pushes a heavy object from an initial position to a desired final position. The following assumptions are made:

1) The location of the robot base can be chosen at the start time, and it is fixed during the task.
2) The contact point between the object and the end effector is modeled as a joint that rotates freely, and the joint is located at the center of mass of the object. Then, the object can be modeled as a mass point.

T. Urakubo, H. Yoshioka and X. Wan are with Graduate School of System Informatics, Kobe University, Kobe, Japan 657–8501 t.urakubo@silver.kobe-u.ac.jp

T. Mashimo is with Electronics Inspired-Interdisciplinary Research Institute, Toyohashi University of Technology, Toyohashi, Japan 441–8580

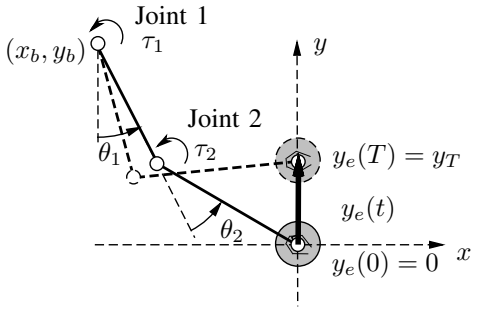

Fig. 1. Two-link robot arm with an object

3) The object is moved along a straight line from the initial position to the final position.

For a mobile manipulator, the first assumption means that the location of the mobile base is chosen and fixed before the start time of the task. Even for an arm on a fixed base, the base location can be chosen in installing it. From the second assumption, we do not have to consider the rotation of the object. Although there are an infinite number of paths of the object that connect an initial position to a final position, the third assumption is appropriate in the absence of obstacles for a sufficiently heavy object.

As shown in Fig. 1, the joint between the robot base and the first link of the arm is called Joint 1, and the joint between the first link and the second link is called Joint 2. We introduce a coordinate frame, (x, y), whose origin is placed on the initial position of the object, and the y axis is set to be along the path to the desired position. The location of the robot base is denoted as $\boldsymbol{p}_b = [x_b, y_b]^T$, and the angles of Joint 1 and 2 are denoted as θ_1 and θ_2 respectively. The input torques at Joint 1 and 2 are expressed as τ_1 and τ_2 respectively. The angles and the torques are represented in vector forms as $\boldsymbol{\theta} = [\theta_1, \theta_2]^T$ and $\boldsymbol{\tau} = [\tau_1, \tau_2]^T$. The position of the end effector of the robot arm is denoted as $\boldsymbol{p}_e = [x_e, y_e]^T$.

In this paper, we examine the optimal base location and arm motion of the two-link robot arm in two cases: *Case A* and *Case B*. In Case A, each link of the robot arm rotates in a horizontal plane, and the object is pulled or pushed horizontally. In Case B, each link of the robot arm rotates in a vertical plane, and the object is lifted up vertically. In both cases, the initial and final positions of the object are set to be $\boldsymbol{p}_e = [0, 0]^T$ and $\boldsymbol{p}_e = [0, y_T]^T$ respectively. Note that the y axis is horizontal in Case A and vertical in Case B. We consider a trajectory that connects those two positions along y axis as in Fig. 1, and denote it as $\boldsymbol{p}_e(t) = [0, y_e(t)]^T$. The conditions on $y_e(t)$ at the start time, $t = 0$, and the end time, $t = T$, are given as follows:

$$(y_e, \dot{y}_e)|_{t=0} = (0, 0) \quad , \quad (y_e, \dot{y}_e)|_{t=T} = (y_T, 0) \ . \tag{1}$$

We introduce the following cost function as a criterion for optimization.

$$J_c(\xi) = \int_{t=0}^{T} (\tau_1^2 + \tau_2^2) dt \ , \tag{2}$$

where ξ represents the parameters for optimization. It is chosen for each case as follows.

$$\text{Case A: } \xi = \{\boldsymbol{p}_b, y_e(t)\} \ , \ \text{Case B: } \xi = \{\boldsymbol{p}_b, y_e(t), T\} \ .$$

In Case B, the end time of lifting up should be included in ξ. The value of the cost function highly depends on the end time because of the gravity. In Case A, after scale transformations of time t and torque $\boldsymbol{\tau}$, we can choose an arbitrary end time T without loss of generality, if no frictional forces exist. Even for the robot arm with frictional forces, we choose T as 0.5 [s] for simplicity.

In this paper, we deal with an optimization problem of finding the parameters that minimize J_c:

$$\xi^* = \arg\min J_c \ . \tag{3}$$

B. Numerical Optimization

The approximate solution for ξ^* will be found by numerical optimization. The trajectory $y_e(t)$ is approximated as fifth order spline functions of time, and the location of the robot base (x_b, y_b) is discretized into a grid. At each grid point, the coefficients of splines that minimize the cost function (2) are found.

The optimal trajectory $y_e(t)$ for a fixed base (x_b, y_b) is searched for as follows. We divide the time interval $[0, T]$ by n and express the trajectory of $y_e(t)$ in each time interval $[t_i, t_{i+1}]$ ($i = 0, \cdots, n-1$ and $t_j = jT/n$ for $j = 0, \cdots, n$) by a fifth order polynomial function of time:

$$\begin{aligned} \varphi_i(t) \ = \ & y_i + b_i(t - t_i) + c_i(t - t_i)^2 + d_i(t - t_i)^3 \\ & + e_i(t - t_i)^4 + f_i(t - t_i)^5 \ , \end{aligned} \tag{4}$$

where y_i, b_i, c_i, d_i, e_i and f_i are scalar parameters. Note that more than fourth order splines for $y_e(t)$ are required to avoid extremely high angular velocities of joints near singular configurations. To make the input torque $\boldsymbol{\tau}$ continuous, we choose the functions $\varphi_i(t)$ such that $\varphi_i(t_{i+1}) = \varphi_{i+1}(t_{i+1})$, $\dot{\varphi}_i(t_{i+1}) = \dot{\varphi}_{i+1}(t_{i+1})$, $\ddot{\varphi}_i(t_{i+1}) = \ddot{\varphi}_{i+1}(t_{i+1})$, for $i = 0, \cdots, n-2$. When the polynomials satisfy those conditions and (1), there are $3n - 1$ independent parameters, and they can be chosen as $\boldsymbol{\Phi} = (y_1, \cdots, y_{n-1}, e_0, f_0, \cdots, e_{n-1}, f_{n-1})$. We assume that $y_e(t)$ monotonically increases at $t = t_i$ and put a constraint that $0 \le y_1 \le \cdots \le y_{n-1} \le y_T$. At each location of the robot base, we search for the values of $\boldsymbol{\Phi}$ in Case A or $(\boldsymbol{\Phi}, T)$ in Case B that minimize the cost function (2), by the Quasi-Newton method.

The grid search method is used to find the optimal base location. The region of (x_b, y_b) defined by $[x_{\min}, x_{\max}] \times [y_{\min}, y_{\max}]$ is divided into a grid, where each rectangle is given by $\Delta x \times \Delta y$. By calculating the minimum value of the cost function at each grid point by the above-mentioned method, we can find the optimal location of the robot base.

In [21], numerical optimization was performed under the assumption that no frictional forces act on the joints or the object. The equation of motion was written as

$$(\boldsymbol{M}(\boldsymbol{\theta}) + m_w \boldsymbol{J}^T \boldsymbol{J})\ddot{\boldsymbol{\theta}} + \boldsymbol{h}(\boldsymbol{\theta}, \dot{\boldsymbol{\theta}}) + m_w \boldsymbol{J}^T \dot{\boldsymbol{J}} \dot{\boldsymbol{\theta}} = \boldsymbol{\tau} + \boldsymbol{\tau}_g(\boldsymbol{\theta}) \, , \tag{5}$$

where the kinetic energy of the two-link arm is expressed as $E_a = (1/2)\dot{\boldsymbol{\theta}}^T \boldsymbol{M}(\boldsymbol{\theta})\dot{\boldsymbol{\theta}}$ by using $\boldsymbol{M}(\boldsymbol{\theta})$, and $\boldsymbol{h}$ is defined as $\boldsymbol{h} = \dot{\boldsymbol{M}}(\boldsymbol{\theta})\dot{\boldsymbol{\theta}} - (\partial E_a/\partial \boldsymbol{\theta})^T$. The term $\boldsymbol{\tau}_g(\boldsymbol{\theta})$ is derived from the potential energy of the arm $P_a(\boldsymbol{\theta})$ as $\boldsymbol{\tau}_g = -(\partial P_a(\boldsymbol{\theta})/\partial \boldsymbol{\theta})^T$, and m_w is the mass of the object. The Jacobian matrix $\boldsymbol{J}$ is defined as

$$\boldsymbol{J} = \begin{bmatrix} l_1 \cos\theta_1 + l_2 \cos(\theta_1 + \theta_2) & l_2 \cos(\theta_1 + \theta_2) \\ l_1 \sin\theta_1 + l_2 \sin(\theta_1 + \theta_2) & l_2 \sin(\theta_1 + \theta_2) \end{bmatrix} , \quad (6)$$

where l_1 and l_2 are the lengths of the first and second links respectively. The matrix provides the kinematic relationship between the end effector position and the joint angles as follows.

$$\dot{\boldsymbol{p}}_e = \boldsymbol{J}\dot{\boldsymbol{\theta}} \ , \ \ddot{\boldsymbol{p}}_e = \boldsymbol{J}\ddot{\boldsymbol{\theta}} + \dot{\boldsymbol{J}}\dot{\boldsymbol{\theta}} \ . \quad (7)$$

When the parameters ξ are given as the spline coefficients and the grid point, the trajectories of joint angles and joint torques, $\boldsymbol{\theta}(t)$ and $\boldsymbol{\tau}(t)$, are calculated from the inverse kinematics and dynamics. The cost function in (2) is also calculated from $\boldsymbol{\tau}(t)$. The numerical results obtained in [21] show that, for the optimized solution, the initial configuration of the robot arm is close to the singular configuration where the arm is stretched out.

III. TWO-LINK ROBOT ARM

In this section, we show the details of the two-link robot arm that is used for the experiments presented later and the equations of motion that are used for numerical optimization.

A. Experimental Setup

The two-link robot arm that was developed for the experiments is shown in Fig. 2. The physical parameters of the robot arm are summarized in Table I.

Fig. 2. Two-link robot arm developed for experiments

TABLE I
PHYSICAL PARAMETERS OF TWO-LINK ROBOT ARM

length of link 1	l_1	0.30 [m]
length of link 2	l_2	0.35 [m]
mass of link 1	m_1	0.342 [kg]
mass of link 2	m_2	0.429 [kg]
inertia of link 1	I_1	0.129 [kgm^2]
inertia of link 2	I_2	0.137 [kgm^2]

Each joint of the arm is driven by a geared DC motor (motor: maxon EC-powermax30, gearhead: maxon GP32HP). The current to each motor is regulated by a motor drive (maxon EPOS) with ROS (Robot Operation System) at 500 Hz.

From the results of preliminary experiments where various sequences of piecewise constant current were applied to each motor, we found that the driving torque $\boldsymbol{\tau}$ is generated from the motor current as follows.

$$\boldsymbol{\tau} = K_e \boldsymbol{i} \ , \quad (8)$$

$$\boldsymbol{i} = [i_1, i_2]^T \ , \quad (9)$$

where i_j is the current to the motor of Joint $j (j = 1, 2)$ and $K_e = 2.5$ [Nm/A]. The frictional torques at the joints were also identified from the preliminary experiments.

$$\tau_{f1} = -0.357\dot{\theta}_1 - 0.238\mathrm{sgn}(\dot{\theta}_1) \ , \quad (10)$$

$$\tau_{f2} = -0.535\dot{\theta}_2 - 0.255\mathrm{sgn}(\dot{\theta}_2) \ , \quad (11)$$

where τ_{fj} acts on Joint $j (j = 1, 2)$ and they are represented in a vector form as $\boldsymbol{\tau}_f$.

B. Equations of Motion

The equation of motion (5) is modified so that several frictional forces for an actual robot arm are included in it. We show the equations for Case A and Case B respectively.

Case A

In the experiments of pulling an object in a horizontal plane, the object was supported in the vertical direction by a ball caster as shown in Fig. 3. For a heavy object, the gravity force acting on the object could overload the shafts of motors without the support caster. The overload is avoided by the floor reaction force through the support caster.

When the object is pulled in the horizontal plane, a frictional force acts at the contact point of the support caster. Then, the equation of motion for the robot arm is rewritten as follows.

$$(\boldsymbol{M} + m_w \boldsymbol{J}^T \boldsymbol{J})\ddot{\boldsymbol{\theta}} + \boldsymbol{h}(\boldsymbol{\theta}, \dot{\boldsymbol{\theta}}) + m_w \boldsymbol{J}^T \dot{\boldsymbol{J}}\dot{\boldsymbol{\theta}} = \boldsymbol{\tau} + \boldsymbol{\tau}_f + \boldsymbol{J}^T \boldsymbol{F}_s \ , \quad (12)$$

where $\boldsymbol{F}_s$ is the frictional force. From the preliminary experiments where various patterns of piecewise constant current were applied for several values of m_w, $\boldsymbol{F}_s$ is approximated as

$$\boldsymbol{F}_s = -0.1425 m_w g \frac{\dot{\boldsymbol{p}}_e}{\|\dot{\boldsymbol{p}}_e\|} \ . \quad (13)$$

In (12), the gravitational torque $\boldsymbol{\tau}_g$ in (5) is eliminated because the potential energy P_a is constant.

Case B

In the experiments of pulling an object in a vertical plane, the support caster is not necessary. The equation of motion for the robot arm is rewritten as follows.

$$(\boldsymbol{M} + m_w \boldsymbol{J}^T \boldsymbol{J})\ddot{\boldsymbol{\theta}} + \boldsymbol{h}(\boldsymbol{\theta}, \dot{\boldsymbol{\theta}}) + m_w \boldsymbol{J}^T \dot{\boldsymbol{J}}\dot{\boldsymbol{\theta}} = \boldsymbol{\tau} + \boldsymbol{\tau}_f + \boldsymbol{\tau}_g \ . \quad (14)$$

By using (12) or (14), the optimization problem in Sec. II-A is solved by the numerical method shown in Sec. II-B.

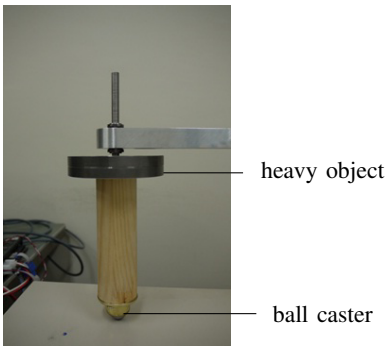

Fig. 3. Support caster for a heavy object (Case A)

IV. EXPERIMENTAL RESULTS

A. Trajectory Tracking

From the motion planning method in Sec. II, we can obtain the planned trajectories of $\boldsymbol{\theta}(t)$ and $\boldsymbol{\tau}(t)$. They are denoted as $\boldsymbol{\theta}_d(t)$ and $\boldsymbol{\tau}_d(t)$ in the rest of the paper. From (8) and $\boldsymbol{\tau}_d(t)$, we can obtain the feedforward signal for motor currents as $\boldsymbol{i} = (1/K_e)\boldsymbol{\tau}_d(t)$.

The feedforward signal is not enough to make the joint angles $\boldsymbol{\theta}$ follow $\boldsymbol{\theta}_d(t)$. Although we modeled the frictional forces at the joints and the support caster as mentioned above, the errors in the models are inevitable. Small delay and error in regulation of motor current by the motor drives also exist.

In order to make $\boldsymbol{\theta}$ follow $\boldsymbol{\theta}_d(t)$ accurately and complete the task, we used the following feedback control law.

$$\boldsymbol{i} = (1/K_e)(\boldsymbol{\tau}_d(t) + \boldsymbol{\tau}_{FB}) \ , \tag{15}$$

$$\boldsymbol{\tau}_{FB} = -c(\dot{\boldsymbol{\theta}} - \dot{\boldsymbol{\theta}}_d) - k(\boldsymbol{\theta} - \boldsymbol{\theta}_d) \ , \tag{16}$$

where the parameters c and k were chosen as $c = 42.42$ [Nms/rad] and $k = 900$ [Nm/rad]. Instead of (16), a more sophisticated feedback controller can be exploited according to the nonlinearity of (12) or (14). The choice of the controller would affect the values of J_c in the experiments. In this paper, a PD controller in the form of (16) is utilized, because it is simple and widely used. The gains c and k were tuned to reduce the tracking error while keeping the stability of the system.

B. Numerical and Experimental Results

In this subsection, we show the results of numerical optimization and experiments with the feedback control. Even under the feedback control, the task of pulling a heavy object is achieved with small joint torques at the optimal base location.

In both Case A and B, the displacement of the object is chosen as $y_T = 0.2$ [m], and the time interval T is divided into four subintervals, that is, $n = 4$. For simulation results, we show the contour plot of the cost function J_c. It can be obtained by finding the optimal value of $\boldsymbol{\Phi}$ or $(\boldsymbol{\Phi}, T)$ at each grid point of the base location.

Case A

In Case A, the mass of the object, m_w, is set to be 7.5 [kg], and the end time T is chosen as 0.5 [s]. From numerical simulations, we obtain the contour plot of J_c as shown in Fig. 4. The grid points of the base location are distributed by choosing Δx and Δy as 0.05 [m], and the minimum value of J_c occurs at the base location denoted as L_0. In order to obtain more accurate solution for the optimal location, we change Δx and Δy to 0.01 [m] and redraw the contour plot of J_c near L_0 as shown in Fig. 5. The obtained solution denoted as L_1 is $(x_b, y_b) = (0.03, 0.64)$ [m]. The value of J_c at L_1 is 6.94 [N^{2}m^{2}s]. As depicted in Fig. 4, the initial posture of the arm for the base location L_1 is close to the singular configuration where the arm is stretched out. At the base locations denoted as S_1 and S_2, the arm is completely stretched out at the start time and the end time respectively. In Fig. 5, the value of J_c decreases as the base location approaches S_1.

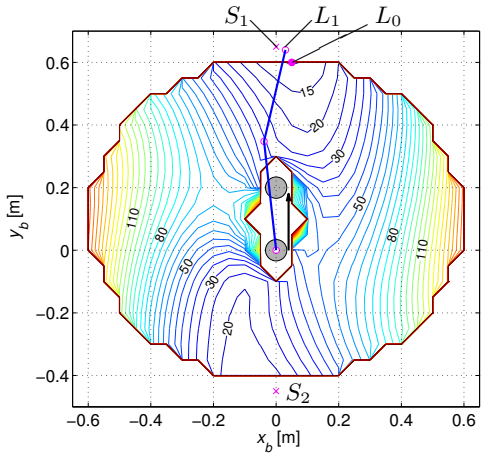

Fig. 4. Cost function for base location (x_b, y_b) (Case A)

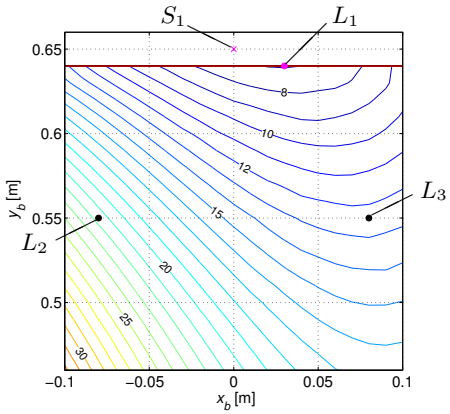

Fig. 5. Cost function for base location (x_b, y_b) near L_0 (Case A)

In order to verify that the values of the cost function near L_1 are small even in the experiments with the feedback control (16), we performed the experiments at three base locations, L_1, L_2 and L_3, which are shown in Fig. 5. The experiments were conducted three times for each base location. The currents to joint motors were measured, and the joint torques were calculated by (8). The obtained values of J_c are summarized in Table. II. Due to the feedback control

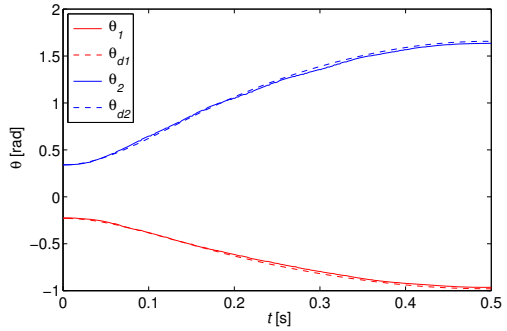

Fig. 6. Time history of joint angles $\boldsymbol{\theta}$ at L_1 (Case A)

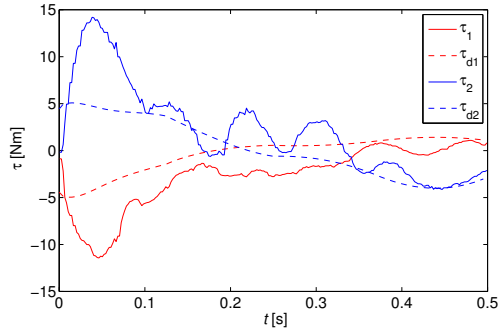

Fig. 7. Time history of joint torque $\boldsymbol{\tau}$ at L_1 (Case A)

(16), the values of J_c for the experiments are larger than the values for numerical simulations. The differences between the values of each experiment for the same location could be caused by small error in initial posture, unsteady friction, and so on. The average value of J_c for the optimal location L_1 is smaller than the average values for L_2 and L_3. For L_1, the joint angles followed the desired angles with small error as shown in Fig. 6. Figure 7 shows the time histories of joint torques $\boldsymbol{\tau}$. They are different from the torques $\boldsymbol{\tau}_d$ planned by numerical simulation, due to the feedback control (16) and error in motor current control.

From the experimental results, the base location close to L_1 is advantageous in reducing the joint torques necessary to achieve the task of pulling a heavy object. It should be noted that, for the base locations where the value of J_c for numerical simulation is much larger, the robot arm could not complete the task because the motor currents reached the upper limit.

TABLE II

THE VALUES OF COST FUNCTION J_c IN EXPERIMENTS (CASE A)

base location	L_1	L_2	L_3
J_c [N^{2}m^{2}s] for numerical simulation	6.936	21.63	12.46
J_c [N^{2}m^{2}s] for 1st experiment	21.73	43.85	28.55
J_c [N^{2}m^{2}s] for 2nd experiment	21.38	46.39	26.71
J_c [N^{2}m^{2}s] for 3rd experiment	21.56	38.69	28.15
Averaged J_c [N^{2}m^{2}s] for the experiments	21.56	45.12	27.63

Case B

In Case B, the mass of the object, m_w, is set to be 2.44 [kg]. Figure 8 shows the contour plot of J_c obtained from numerical simulation, where Δx and Δy are chosen as

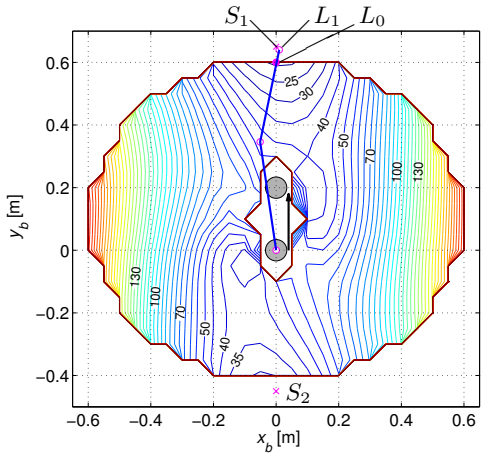

Fig. 8. Cost function for base location (x_b, y_b) (Case B)

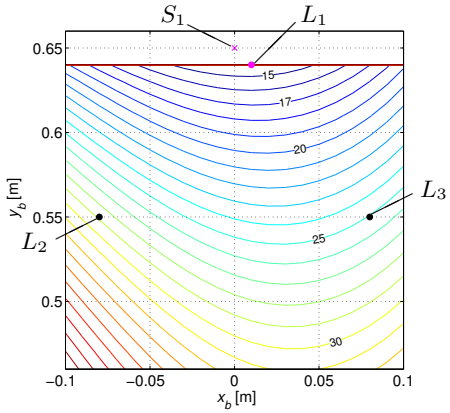

Fig. 9. Cost function for base location (x_b, y_b) near L_0 (Case B)

0.05 [m]. More accurate solution for the optimal location is obtained from the contour plot near L_0 where $\Delta x = \Delta y = 0.01$ [m] (Fig. 9). The obtained solution denoted as L_1 is $(x_b, y_b) = (0.01, 0.64)$ [m]. The value of J_c at L_1 is 14.12 [N^{2}m^{2}s], and the end time T is 0.417 [s]. As depicted in Fig. 8, the initial posture of the arm for the base location L_1 is close to the singular configuration where the arm is stretched out.

The experiments with the feedback control (16) were performed at three base locations as well as in Case A. Those locations are shown as L_1, L_2 and L_3 in Fig. 9. The experiments were repeated three times for each base location, and the values of J_c were calculated from the measured currents to joint motors. The obtained values of J_c are summarized in Table. III. The differences between the values for the same location could happen for the same reasons as in Case A. The average value of J_c for the optimal location L_1 is smaller than the average values for L_2 and L_3.

The experimental results show that the base location close to L_1 is advantageous in reducing the joint torques necessary to achieve the task of lifting a heavy object up. As well as in Case A, for the base locations where the value of J_c for numerical simulation is much larger, the robot arm could not complete the task because of the motor current limit.

TABLE III

THE VALUES OF COST FUNCTION J_c IN EXPERIMENTS (CASE B)

base location	L_1	L_2	L_3
J_c [N^2m^2s] for numerical simulation	14.12	28.83	25.08
J_c [N^2m^2s] for 1st experiment	23.57	45.96	41.43
J_c [N^2m^2s] for 2nd experiment	23.96	45.29	41.32
J_c [N^2m^2s] for 3rd experiment	24.25	44.86	41.22
Averaged J_c [N^2m^2s] for the experiments	23.77	45.63	41.38

C. Discussion

At a singular configuration, the Jacobian matrix $\boldsymbol{J}$ in (6) is singular, and it can be shown from (5) that the joint angle vector $\boldsymbol{\theta}$ can be accelerated in a certain direction almost independently of the mass of the object. Consequently, the kinetic energy of the arm can be generated with small joint torques, and it can be used to pull or lift up the object theoretically [21]. The results of the experiments with a feedback control show that utilization of this dynamic feature of singular configuration is practically feasible.

For practical tasks, the trajectory of the object during pulling or lifting up it does not have to be restricted to being on a straight line. The optimal motion planning problem in Sec. II can be solved in the same manner even when the trajectory of $x_e(t)$ is not restricted to being constant. The trajectory of $x_e(t)$ can be expressed by spline functions, and the coefficients of splines can be included in $\boldsymbol{\Phi}$ in Sec. II-B. The results of numerical simulations show that the obtained trajectory of the object at the optimal base location follows closely the straight line where $x_e = 0$. In this paper, we showed the results where the trajectory is restricted on $x_e = 0$ for simplicity of the presentation.

When a robot arm pulls or lifts up an unknown object in a certain direction, the motion cannot be planned in advance by the method in Sec. II-B. However, the results of the paper show that, for a heavy object, the base location should be chosen to be close to the one where the robot arm is stretched out in the direction of pulling at the start time. As mentioned above, there exists the direction of joint angle acceleration that does not depend on the mass of the object. The direction of joint torque vector corresponding to the acceleration is determined only by the lengths of two links [21]. Therefore, the task of pulling or lifting up a heavy object would be able to be done by using the joint torque in that direction with a feedback control. Otherwise, the mass of an object could be estimated by several trials of moving the object.

V. CONCLUSIONS

In this paper, we demonstrated that a singular configuration of a two-link robot arm is advantageous in pulling and lifting up a heavy object with small joint torques. Even when a feedback control is applied to make the end effector follow the planned trajectory, the experimental results show that the initial configuration at the optimal base location that minimizes the joint torques is close to a singular configuration. Our future work will investigate the dynamic feature of singular configurations for multi-body systems that have more than three links.

ACKNOWLEDGMENT

This work was supported by KAKENHI (23760230, Grant-in-Aid for Young Scientists (B)).

REFERENCES

[1] B. J. Martin and J. E. Bobrow, "Minimum-Effort Motions for Open-Chain Manipulators with Task-Dependent End-Effector Constraints," *The International Journal of Robotics Research*, vol. 18, no. 2, pp. 213-224, 1999

[2] T. Yoshikawa, "Manipulability of Robotic Mechanisms," *The International Journal of Robotics Research*, vol. 4, no. 2, pp. 3-9, 1985

[3] C. Gosselin and J. Angeles, "Singularity Analysis of Closed-Loop Kinematic Chains," *IEEE Trans. on Robotics and Automation*, vol. 6, no. 3, pp. 281-290, 1990

[4] F. C. Park and J. W. Kim, "Singularity Analysis of Closed Kinematic Chains," *ASME Journal of Mechanical Design*, vol. 121, no. 1, pp. 32-38, 1999

[5] J. T. Wen and L. S. Wilfinger, "Kinematic Manipulability of General Constrained Rigid Multibody Systems," *IEEE Trans. on Robotics and Automation*, vol. 15, no. 3, pp. 558-567, 1999

[6] O. Altuzarra, C. Pinto, R. Avilés and A. Hernández, "A Practical Procedure to Analyze Singular Configurations in Closed Kinematic Chains," *IEEE Trans. on Robotics*, vol. 20, no. 6, pp. 929-940, 2004

[7] L. Nielsen, C. Canudas de Wit and P. Hagander, "Controllability Issues of Robots in Singular Configurations," *Proc. of IEEE Conference on Robotics and Automation*, 1991, pp. 2210-2215

[8] M. Sampei and K. Furuta, "Robot Control in the Neighborhood of Singular Points," *IEEE Journal of Robotics and Automation*, vol. 4, no. 3, pp. 303-309, 1988

[9] J. Kieffer, "Differential Analysis of Bifurcations and Isolated Singularities for Robots and Mechanisms," *IEEE Trans. on Robotics and Automation*, vol. 10, no. 1, pp. 1-10, 1994

[10] D. N. Nenchev, Y. Tsumaki and M. Uchiyama, "Singularity-Consistent Parameterization of Robot Motion and Control," *The International Journal of Robotics Research*, vol. 19, no. 2, pp. 159-182, 2000

[11] Y. Nakamura and H. Hanafusa, "Inverse Kinematic Solutions With Singularity Robustness for Robot Manipulator Control," *ASME Journal of Dynamic Systems, Measurement, and Control*, vol. 108, no. 3, pp. 163-171, 1986

[12] C. W. Wampler II and L. J. Leifer, "Applications of Damped Least-Squares Methods to Resolved-Rate and Resolved-Acceleration Control of Manipulators," *ASME Journal of Dynamic Systems, Measurement, and Control*, vol. 110, no. 1, pp. 31-38, 1988

[13] K.-S. Chang and O. Khatib, "Manipulator Control at Kinematic Singularities: A Dynamically Consistent Strategy," *Proc. of IEEE/RSJ International Conference on Intelligent Robots and Systems*, 1995, pp. 84-88

[14] O. Khatib, "A Unified Approach for Motion and Force Control of Robot Manipulators: The Operational Space Formulation," *IEEE Journal of Robotics and Automation*, vol. 3, no. 1, pp. 43-53, 1987

[15] V. M. Zatsiorsky, "Kinematics of Human Motion," Human Kinetics, 1998

[16] J. Lenarčič and L. Žlajpah, "Control Considerations on Minimum Joint Torque Motion," *Lecture Notes in Control and Information Sciences*, vol. 200, pp. 40-49, 1994

[17] V. Kumar and J. F. Gardner, "Kinematics of Redundantly Actuated Closed Chains," *IEEE Trans. on Robotics and Automation*, vol. 6, no. 2, pp. 269-274, 1990

[18] K. H. Hunt, "Special Configurations of Robot-arms via Screw Theory," *Robotica*, vol. 4, issue 3, pp. 171-179, 1986

[19] S. B. Nokleby and R. P. Podhorodeski, "Pose Optimization of Serial Manipulators Using Knowledge of Their Velocity-Degenerate (Singular) Configurations," *Journal of Robotic Systems*, vol. 20, no. 5, pp. 239-249, 2003

[20] K. L. Brown, "Design and Analysis of Robots that Perform Dynamic Tasks Using Internal Body Motion," *Ph.D. Thesis*, MIT, 1994

[21] T. Urakubo, T. Mashimo and T. Kanade, "Efficient Pulling Motion of a Two-Link Robot Arm near Singular Configuration," *Proc. of IEEE/RSJ International Conference on Intelligent Robots and Systems*, 2010, pp.1372-1377